Development of a high-resolution cavity-beam position monitor

著者	Inoue Yoichi, Hayano Hitoshi, Honda Yosuke, Takatomi Toshikazu, Tauchi Toshiaki, Urakawa Junji, Komamiya Sachio, Nakamura Tomoya, Sanuki Tomoyuki, Kim Eun-San, Shin Seung-Hwan, Vogel Vladimir
journal or publication title	Physical Review. Special Topics. Accelerators and Beams
volume	11
number	6
page range	062801
year	2008
URL	http://hdl.handle.net/10097/52566

doi: 10.1103/PhysRevSTAB.11.062801

Development of a high-resolution cavity-beam position monitor

Yoichi Inoue
Tohoku Gakuin University, Sendai, Miyagi, Japan

Hitoshi Hayano, Yosuke Honda,* Toshikazu Takatomi, Toshiaki Tauchi, and Junji Urakawa
High Energy Accelerator Research Organization (KEK), Tsukuba, Ibaraki, Japan

Sachio Komamiya, Tomoya Nakamura, and Tomoyuki Sanuki†
University of Tokyo, Hongo, Tokyo, Japan

Eun-San Kim and Seung-Hwan Shin
Kyungpook National University, Daegu, Korea

Vladimir Vogel
Deutsches Electronen-Synchrotron, Hamburg, Germany
(Received 31 December 2007; published 16 June 2008)

We have developed a high-resolution cavity-beam position monitor (BPM) to be used at the focal point of the ATF2, which is a test beam line that is now being built to demonstrate stable orbit control at ~nanometer resolution. The design of the cavity structure was optimized for the Accelerator Test Facility (ATF) beam in various ways. For example, the cavity has a rectangular shape in order to isolate two dipole modes in orthogonal directions, and a relatively thin gap that is less sensitive to trajectory inclination. A two stage homodyne mixer with highly sensitive electronics and phase-sensitive detection was also developed. Two BPM blocks, each containing two cavity BPMs, were installed in the existing ATF beam line using a rigid support frame. After testing the basic characteristics, we measured the resolution using three BPMs. The system demonstrated 8.7 nm position resolution over a dynamic range of 5 μm.

DOI: 10.1103/PhysRevSTAB.11.062801 PACS numbers: 29.27.Eg, 41.85.Qg, 41.20.−q

I. INTRODUCTION

Future accelerators, such as linear colliders (LC) and x-ray free electron lasers, will require precise beam handling. High-resolution beam position measurement is the key to precise beam handling. An rf cavity-type beam position monitor (cavity BPM) may be able to measure the beam position at ~nanometer resolution. It has been studied in various places [1–4].

The Accelerator Test Facility (ATF) [5] at the High Energy Accelerator Research Organization (KEK) is an ideal place to develop a beam diagnostic device as its extraction line can provide a low emittance beam via radiation damping in the damping ring. The beam energy is 1.3 GeV. The nominal beam charge is 10^{10} electrons/bunch. The typical bunch at nominal charge in the extraction line is 100 μm horizontally, 10 μm vertically, and about 8 mm longitudinally. The beam repetition rate is 1.5 Hz under normal operating conditions.

An extension of the existing extraction line, called the ATF2 [6], is under construction. It will be a test beam line for the final focusing system of the LC. The main goals of the ATF2 project are to prove the possibility of focusing the beam down to ~nanometer size while stabilizing beam position to within ~nanometers. Although a beam position monitor (BPM) with nanometer resolution is not required for the LC's final focusing system, it plays important roles specific to the focal point (the virtual IP) of the ATF2 project. It provides a direct demonstration of beam position stability at the IP, tracks the beam trajectory during beam size measurements to correct the effects of position jitter, and produces a feedback signal to stabilize the beam orbits of the following bunches. We have developed a new cavity BPM for the IP-BPM of the ATF2 and tested its performance in the existing ATF extraction line.

This paper summarizes the principles of cavity BPMs, then explains the design of the new cavity BPM. The paper reports the basic characteristics as determined by beam tests, describes the high sensitivity electronics and resolution measurements, and discusses the results.

II. PRINCIPLE OF CAVITY BPMS

A. Excitation of a cavity by a beam

Interaction of a charged particle in a beam and the cavitylike structure in a beam duct is characterized by the normalized shunt impedance (R/Q) of the cavity eigenmode of interest as defined below:

*Corresponding author.
yosuke@post.kek.jp
†Present address: Tohoku University, Sendai, Miyagi, Japan.

$$R/Q = \frac{|\int \vec{E} d\vec{s}|^2}{\omega U}, \tag{1}$$

where ω is the angular frequency, U is the energy excited in the cavity, and the numerator indicates integration of the electric field of the mode along the beam passage. The excited energy in the cavity by a beam bunch is calculated using the following equation:

$$U = \frac{\omega}{4}(R/Q)q^2 \exp\left(-\frac{\omega^2\sigma_z^2}{c^2}\right), \tag{2}$$

where c is the speed of light, q is the bunch charge, and σ_z is the rms bunch length of the Gaussian distribution. The energy in a cavity and the power that streams out from a readout port (P_{out}) are connected via a parameter called the external quality factor (Q_{ext}),

$$Q_{\text{ext}} = \frac{\omega U}{P_{\text{out}}}. \tag{3}$$

Detecting the power with an impedance Z, the measured voltage at the end (V_{out}) is calculated as

$$V_{\text{out}} = \frac{\omega q}{2}\sqrt{\frac{Z}{Q_{\text{ext}}}(R/Q)}\exp\left(-\frac{\omega^2\sigma_z^2}{2c^2}\right). \tag{4}$$

A more detailed discussion of the theory can be found elsewhere [7].

In the vicinity of the node points of an antisymmetric mode, E behaves as a linear function of the transverse position. This results in a linear response of V_{out} to a function of the transverse beam position of the beam. Hence, it can be used as a beam position monitor. A dipole mode is a natural solution for such modes. Here, we describe an example calculation of a cylindrical cavity of diameter a and length L. The bottom figure of Fig. 1 shows the field shapes of the dipole mode in the cavity. The electrical field is oriented in the z direction and can be written as follows:

$$E_z = E_0 \sin(\phi) J_1(rk_{11}) e^{i\omega_{11}t} \tag{5}$$

$$k_{11} = \omega_{11}/c = j_{11}/a, \tag{6}$$

where J_m is the Bessel function of mth order. j_{mn} is the n root of J_m, and j_{11} is about 3.83. The R/Q of the beam orbit at $r = y$ and $\phi = \pi/2$ is calculated as follows:

$$R/Q(y) = \frac{2J_1^2(yk_{11})LT^2}{\omega_{11}\epsilon_0\pi\frac{a^2}{2}J_0^2(ak_{11})}, \tag{7}$$

where $T = \frac{\sin(\omega_{11}L/2c)}{\omega_{11}L/2c}$, and ϵ_0 is the permittivity of free space. The following is an approximation of $J_1(yk_{11}) \approx yk_{11}/2$ ($yk_{11} \ll 1$):

$$R/Q = 50.5 \times \left(\frac{\omega_{11}}{c}\right)^3 LT^2y^2. \tag{8}$$

As seen in Eq. (4), V_{out} is proportional to the square root of

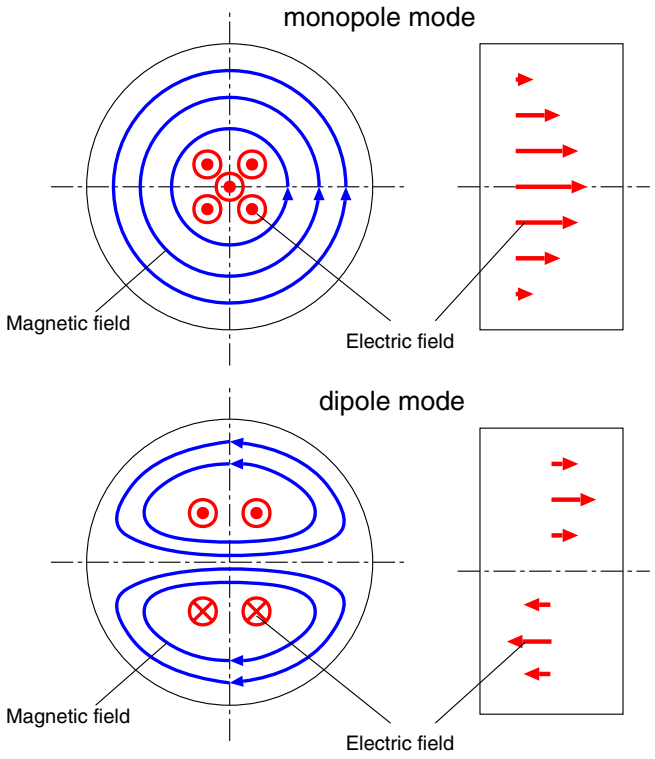

FIG. 1. (Color) First two eigenmodes, TM_{010} (monopole mode) and TM_{110} (dipole mode), of a cylindrical cavity.

R/Q. The signal amplitude is proportional to the beam charge and the transverse distance of beam from the center, and its phase flips at the center. On the other hand, a monopole mode has no beam position sensitivity near its center. It produces a signal with amplitude proportional to the beam charge and its phase is determined by the beam arrival time. Combining the measurements for the dipole and monopole mode cavities, it is possible to calculate the beam position. There are two dipole modes one with x polarization and one with y polarization. The bottom figure in Fig. 1 shows the dipole mode with y polarization, which is sensitive to beam position in the y direction. The two polarizations must be isolated to accurately measure the two-dimensional beam position. We chose a rectangular cavity shape for this study since it explicitly changes the resonance frequency of the two dipole modes. The principle of beam position detection also holds.

B. Properties of beam signal

Even if the beam passes through the center of the cavity, there are other mechanisms to excite a dipole mode. When the beam trajectory has the angle illustrated in Fig. 2, it produces a dipole mode but in the quadrature phase with respect to the case of a parallel offset. The situation can be understood as follows. The inclined trajectory can be modeled as the broken line in the figure. The excited signal of a beam with parallel trajectory of offset x is written as

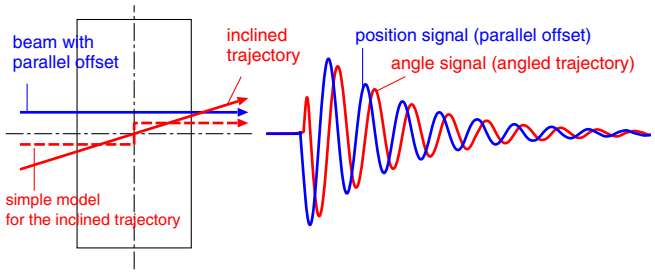

FIG. 2. (Color) Signal of inclined trajectory. The parallel offset of beam orbit and inclined orbit excites the same dipole mode but in a 90-degree different phase.

follows:

$$\text{position signal}\,(x) = Ax\sqrt{L}\sin(\omega t). \tag{9}$$

In this case, the excited signal of a beam with the inclined trajectory of angle x' can be written as follows:

$$\text{angle signal}(x') = Ax'\frac{L}{4}\sqrt{\frac{L}{2}}\sin[\omega(t + L/4c)] - Ax'\frac{L}{4}\sqrt{\frac{L}{2}}\sin[\omega(t - L/4c)] \tag{10}$$

$$= Ax'\frac{L}{2}\sqrt{\frac{L}{2}}\sin(\omega L/4c)\cos(\omega t). \tag{11}$$

Most of the voltage produced in the upstream half of the cavity is canceled by the voltage produced in the downstream half. However, the phase shift due to the transit time that corresponds to half the length of the cavity leaves part of the signal uncanceled. The voltage of this signal is proportional to the trajectory angle and it is in the quadrature (90-degree difference) phase. Its sensitivity is basically proportional to the square of the cavity length.

The longitudinal tilt of a bunch (y-z correlation) [8] or the frequency tail portion of a common-mode signal [2] also can produce the quadrature-phase component of the dipole mode frequency. Avoiding contamination of these components and measuring the actual position of a beam requires a phase-sensitive detection scheme.

III. DESIGN AND FABRICATION OF THE CAVITY BPM

A. Design of the BPM cavity

The first step in designing a cavity BPM is to determine the structure for selectively reading out a dipole mode signal [9]. We adopted a magnetic coupling scheme through slots located in the cavity's end plate. This is basically the same scheme used by other cavity BPMs studied at the ATF [4].

In general, when the bunch length is sufficiently shorter than the wavelength of the rf, positional sensitivity increases as the frequency of the cavity increases. However, the relatively long bunch length at the ATF is less sensitive at higher frequencies as seen by the exponential factor in Eq. (4). Frequencies in the C-band seem to be optimal in our case. The bunch timing in the extraction line should be synchronized to the rf of the damping ring accelerator cavity, which operates at 714 MHz. The harmonics of the frequency have some advantages as the dipole modes of our BPM. For example, they simplify the electronics needed to detect a locked beam, adding up multibunch signal in phase enables us to measure the average beam position of a bunch train in future fast multibunch operations.

Isolation of two dipole modes is an issue in the case of cylindrical cavity because the two modes are degenerated in frequency. Since we should be able to measure a small signal of vertical position in a relatively unstable orbit in horizontal plane at the special beam optics of the IP area, we preferred explicit X-Y isolation and selected a rectangular shape. The frequency of the two dipole modes are 6.426 and 5.712 GHz for the y and x dipole modes, respectively. It perfectly isolates the two modes.

The strong focusing optics at the IP converts the incoming beam jitter into trajectory angle jitter. The angle signal of the dipole mode may contaminate the position measurement due to imperfect phase detection. Usually, the length of the main cavity in the beam direction is designed to maximize the position sensitivity. The optimum length is determined by the frequency and transit time. Since the sensitivity to the trajectory angle is basically proportional to the square of the effective length of the main cavity, we chose a shape that is thinner than usual for the angle signal reduction.

For the thin cavity to have the sensitivity for measurements to within a few nanometers, the beam aperture had to be reduced to increase the R/Q. The beam aperture has a racetrack shape $\phi 6$ mm in height and $\phi 12$ mm in width. Independently calculating the numerator and denominator of Eq. (1) for the dipole mode using MAFIA [10], the R/Q of a given orbit can be estimated. It was calculated to be 0.549 Ω and 1.598 Ω, respectively, for a beam orbit offset by 1 mm in the X and Y directions.

The dimensions of the coupling slots determine Q_{ext} and control the height of the signal peak. Although a higher coupling increases the sensitivity, it also reduces the dynamic range by saturating the detection electronics. We set our targets for β, the ratio of the energy that coupled out and consumed in the cavity, to 1.4 for X port and 2.0 for Y port.

The waveguide is designed to reject the lowest order common mode. The width of the waveguide is set so that the cutoff frequency is between the dipole modes and the common mode. The signal is picked up by the coaxial cable at the electrical antenna placed near the end of the waveguide. Reflections due to imperfect matching at the

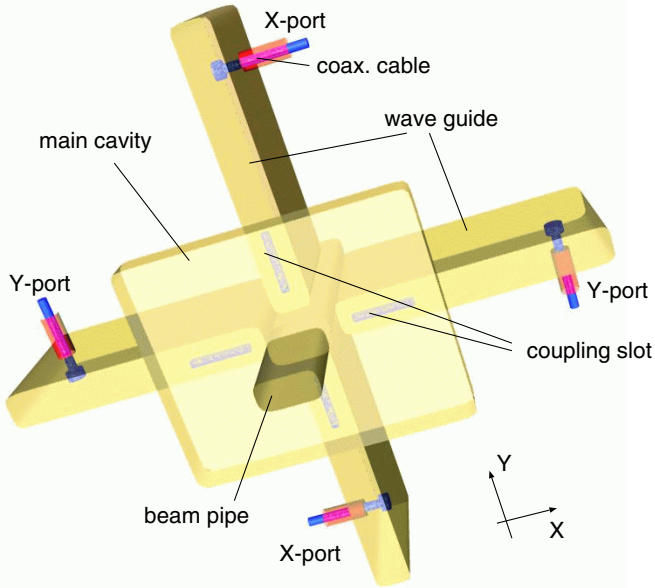

FIG. 3. (Color) Structure of the BPM cavity.

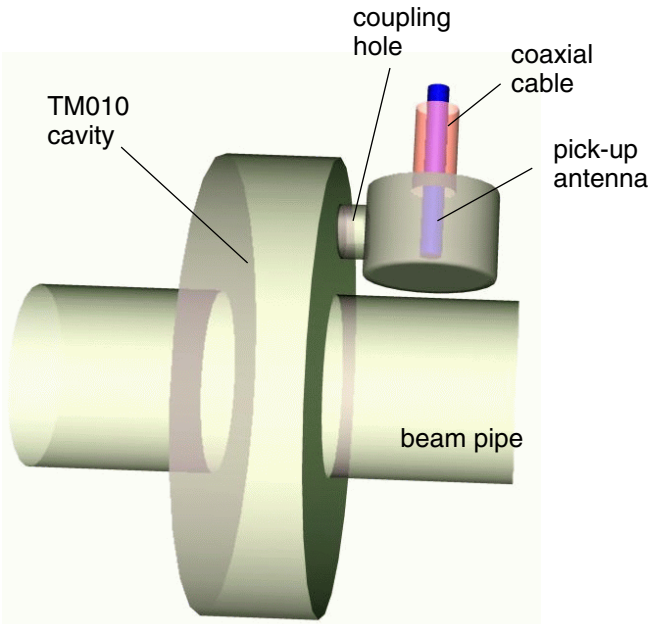

FIG. 4. (Color) Structure of the reference cavity.

antenna may excite a standing wave mode in the waveguide. The length of the waveguide is set so that the dipole mode frequency does not coincide with the waveguide modes.

The structure of the BPM cavity is illustrated in Fig. 3. The four output ports do not break the symmetry of the shape. The waveguides that extend in the x direction are for reading out the y dipole mode (Y port), while those extending in the y direction are for reading out the x dipole mode (X port). The signals from the two ports for the same mode contain basically the same information but have an opposite phase.

B. Design of the reference cavity

To obtain the phase reference and measure the beam charge, the cylindrical cavities were designed with the lowest symmetric mode, TM_{010}, and the same frequencies as the dipole modes of the BPM cavity. Since excitation of the lowest symmetric mode dominates all modes, no special selective coupler is needed. As shown in Fig. 4, the signal is coupled out to a coaxial cable through a small coupling hole in the end plate. Two reference cavities corresponding to the BPM cavity's two dipole mode frequencies were made.

C. Fabrication and bench tests

Measurement of the beam position at two locations in a drift space can determine the beam orbit. The BPM block contains two BPM cavities to fix the relative position of the two. The BPM block consists of five copper parts, SMA feedthroughs for signal pickup, and International Conflat Flange (ICF) flanges for connection to the beam duct. The rectangular main cavity and four waveguides were shaped

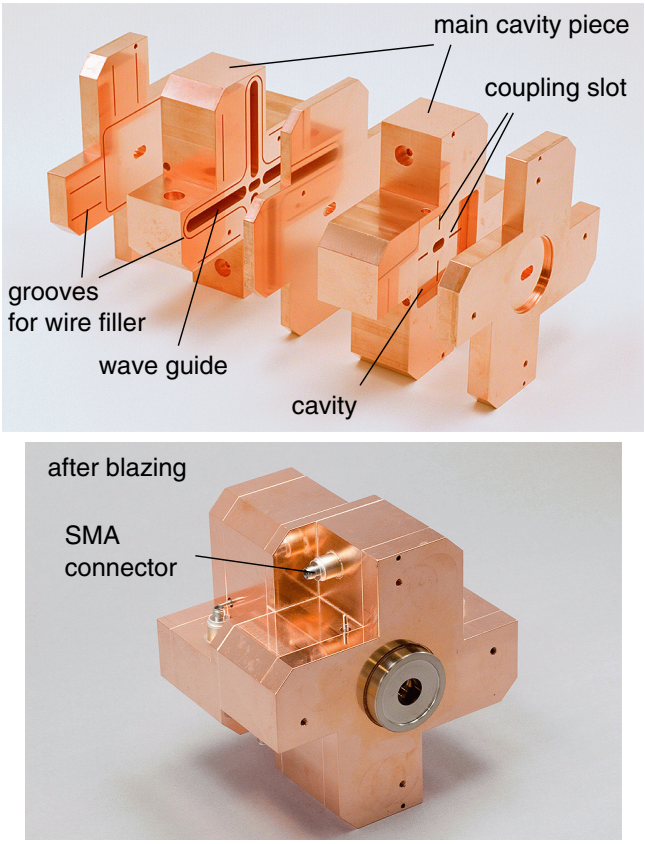

FIG. 5. (Color) Fabrication of the BPM block. A BPM block, which contains two cavities, is made by stacking 5 copper pieces. The copper pieces and SMA connectors were attached by a brazing process as shown in the bottom figure (ICF flanges are not yet attached in this picture).

TABLE I. The rf measurement results of cavity BPMs. (Since there are two blocks and each contains two cavities, they are identified as block_no.-cavity_no.).

BPM (port)	f_0 (GHz)	β	Q_L	Q_0	Q_{ext}
1-1 (X)	5.7073	1.38	2146	5116	3695
1-1 (Y)	6.4202	3.03	1200	4834	1595
1-2 (X)	5.7075	1.32	2174	5036	3826
1-2 (Y)	6.4217	2.66	1304	4777	1793
2-1 (X)	5.7083	1.28	2222	5059	3962
2-1 (Y)	6.4206	2.20	1568	5014	2281
2-2 (X)	5.7076	1.38	2171	5177	3739
2-2 (Y)	6.4208	2.97	1100	4366	1470
Simulation (X)	5.7086	1.63	2062	5424	3335
Simulation (Y)	6.4336	3.32	1217	5459	1586

by machining the main copper piece from both ends. Four coupling slots were fabricated using electric discharge machining . The precision of each machined piece was checked using a coordinate measuring machine (CMM), which confirmed a machining accuracy of about 20 μm. Since each block contained two cavity BPMs, there are two such main pieces and three end plates, as shown in Fig. 5. To accommodate wire fillers for brazing the pieces, grooves were cut into connection surfaces. The five pieces were first brazed with Au filler, and then the SMA feedthroughs with a pickup antenna were brazed at a lower temperature. Finally, an ICF flange was welded to each end.

The properties of the completed cavities were measured port-to-port using a network analyzer. From the measurements of the resonant curve's peak frequency, height/depth, and width, we extracted basic parameters, such as the resonance frequency of the dipole modes (f_0), the coupling strength (β), the loaded quality factor (Q_L), the internal quality factor (Q_0), and the external quality factor (Q_{ext}). The results are summarized in Table I, which also shows the HFSS [11] simulation results.

The reference cavity was fabricated in a similar way. Table II summarizes the rf measurements. Frequency tuner ports were installed in the reference cavities to push/pull the rim wall of the cavities. After installed in the beam line, the frequency of the reference cavity was adjusted to within ± 500 kHz of the dipole mode frequency of the BPM cavity.

TABLE II. The rf measurement results of reference cavities (measurement before installation).

Reference cavity	f_0 (GHz)	β	Q_L	Q_0[a]	Q_{ext}
For X ports	5.7085	0.0080	8249	8315	1 043 525
For Y ports	6.4205	0.0105	6979	7052	670 836
Simulation (for X)	5.5367	0.0177	7400	7530	425 055
Simulation (for Y)	6.3823	0.0176	7450	7581	431 359

[a]It appears that the measured number of Q_0 is higher than the simulated one. It is not an usual case of rf cavity. We guess accuracy of our measurement of Q_0 may be worse in the case of very small β as this one due to difficulty in determining the resonant width on a baseline with some variation of calibration imperfection.

IV. INSTALLATION AND BASIC TESTS

A. Installation

Testing a very high-resolution BPM using a large beam trajectory jitter generally entails three samples from the BPM. The intrinsic position resolution can be estimated by comparing the beam orbit tracked by two of the samples with the measured beam orbit tracked by the remaining sample. The mounting frame of the three BPM system must be rigid enough to remain unaffected by mechanical instability. We made a test area in the last section of the extraction line, where the temperature is passively stabilized to limit variation to within 10 mK, and the ground vibration is isolated by a heavy granite table. A BPM support system with two mounted BPM blocks was installed, as shown in Fig. 6. We used three cavities (labeled 1, 2, and 3 in the figure) out of the total of four available due to limited electronics. To avoid loss of mechanical rigidity, the system did not include a mover mechanism to change the relative positions of the blocks. Since BPMs have limited dynamic range, the centers of all BPMs must be precisely aligned along a straight line to within a few μm. The relative misalignment measured from the beam

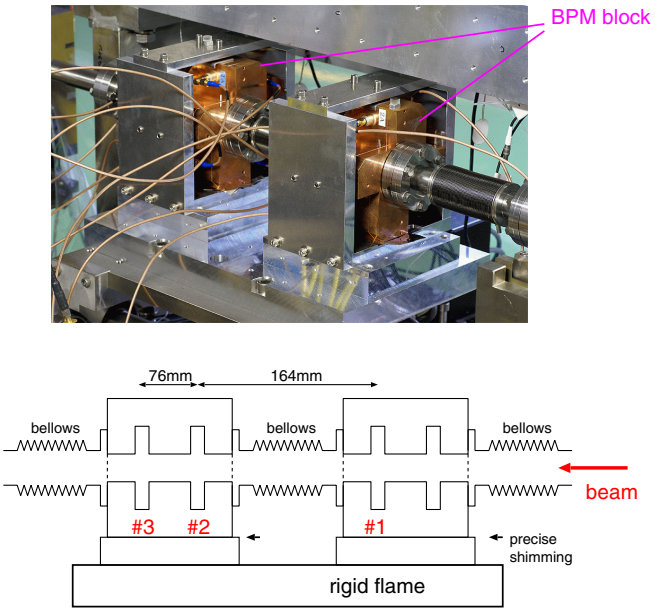

FIG. 6. (Color) BPM support system installed in the beam line. Two blocks were rigidly mounted in the system. The three cavities named 1, 2, and 3 were used in this test. Distances between cavities were 164 and 76 mm. They determine the geometrical factor that appears in the resolution analysis to be 0.799.

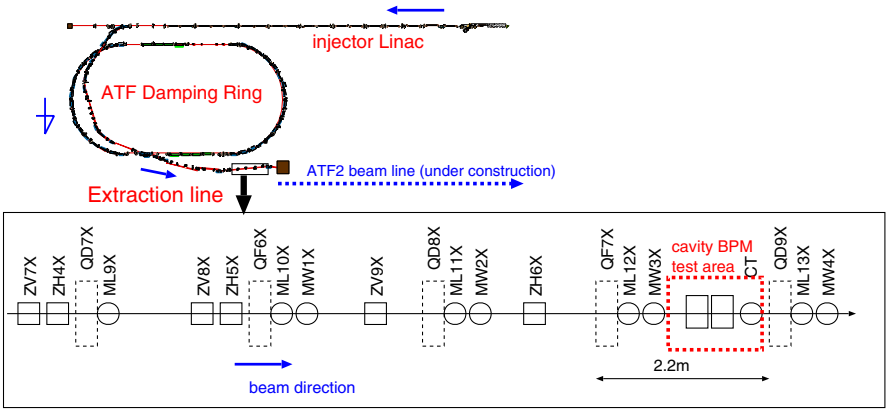

FIG. 7. (Color) Beam line layout near the cavity BPM system. QDnX and QFnX are quadrupole magnets. MLnX are stripline BPMs attached on quadrupole magnets. ZVnX and ZHnX are steering magnets for the vertical and the horizontal direction, respectively. MWnX are wire scanners.

signal in the initial installation was precisely corrected by inserting spacers between the mount frame and the BPMs.

B. Devices in the beam line

The layout of the beam line is shown in Fig. 7. The beam positions were controlled with steering magnets and monitored with stripline BPMs on each quadrupole magnet. Wire scanners [12] were usually used to measure transverse beam profiles and to check beam optics. To simplify the beam optics in our experiment, the quadrupole magnets in this region were turned off.

Since the position sensitivity of the cavity BPMs must be calibrated with respect to other devices, the stripline BPMs must be absolutely precise. The strength of the steering magnets and the sensitivity factor of the stripline BPMs were checked prior to our experiments, Wire scanners, which can directly sense the beam position, were used to determine an absolute position reference. The strength of the kick and the sensitivity factor of the stripline BPM were measured by changing the current of a steering magnet while tracking the actual beam position with wire scanners in the downstream and stripline BPMs. The absolute precision of the calibration procedure was estimated to be 2.5%, which was included in the systematic error of the final result for BPM resolution.

C. Position sensitivity test

First, we checked the sensitivity to beam position—how much power a known beam offset produced. The combined signal from two opposite ports of the BPM was detected with some simple electronics (Fig. 8), which measured the amplitude of the signal within the frequency region near the dipole mode without detecting phase information. The overall sensitivity of the electronics had been calibrated in advance using a cw signal source and a spectrum analyzer. The peak height of the output while changing the beam orbit with steering magnets was measured (Fig. 8). The abscissa is the beam position at the cavity BPM as interpolated from the nearest stripline BPMs. The ordinate is the signal voltage at the port of the BPM normalized to 10^{10} electrons/bunch. Since this detection scheme ignores the phase information, the data plot is V shaped with the minimum at the electrical center of the cavity. The slope of the V shape corresponds to the sensitivity. The expected lines calculated by Eq. (4) are also shown in Fig. 8.

D. Angle sensitivity test

To measure the signal produced by the trajectory angle, the following experiment was carried out. Instead of inclining the beam orbit, the BPM block was mechanically tilted to a large angle with respect to the beam direction.

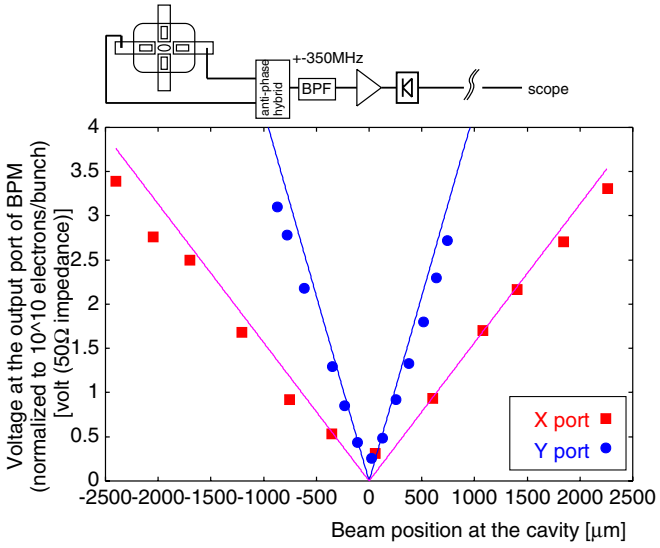

FIG. 8. (Color) The result of position sensitivity measurement. Signals from two opposite ports were combined with an anti-phase hybrid. It was measured with the simple electronics illustrated in the top. Sensitivity can be measured from the slope of the V shape. Lines are the expectation from the cavity design.

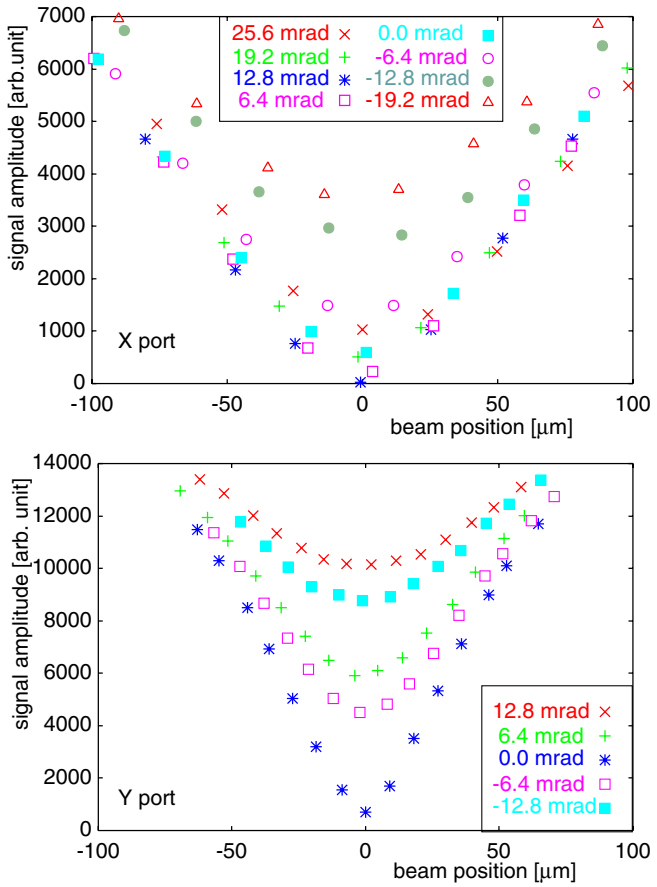

FIG. 9. (Color) The result of angle sensitivity measurement. The top and the bottom plots are the data of the X direction and the Y direction, respectively.

The signal amplitude was measured as a function of the beam position in the same manner as done for the position sensitivity test. The results for various block tilt angles are shown in Fig. 9. Since the trajectory angle produces a signal independent of the beam position, the signal never becomes zero even if the beam is centered in the cavity. The offset of the minimum in the plots was used to estimate how much position signal corresponds to the angle signal. The 1 mrad of angle signal corresponded to 2 and 4 μm of position signal in the X and Y directions, respectively. The high gain electronics to measure a few nm position have a limited dynamic range of about 5 μm. Thanks to the angle signal reduction, a large beam angle jitter in the IP area, which is expected to be about 100 μ rad in our case, does not invalidate the measurement.

V. ELECTRONICS

A. Scheme of the electronics

A schematic diagram of the electronics is shown in Fig. 10. Although it shows only the Y ports of one BPM, the X ports are processed similarly and all of the BPMs are the same.

Signals from two output ports for the same information (X ports or Y ports) are fed into an antiphase hybrid through a pair of matched-length cables. This increases the signal by 3 dB, and simultaneously cancels unwanted signals in the in-phase. After combining the two signals, a bandpass filter (BPF) of $\pm$350 MHz bandwidth (BW) is added in order to reject the other modes. A variable attenuator switches the sensitivity during beam operation. The

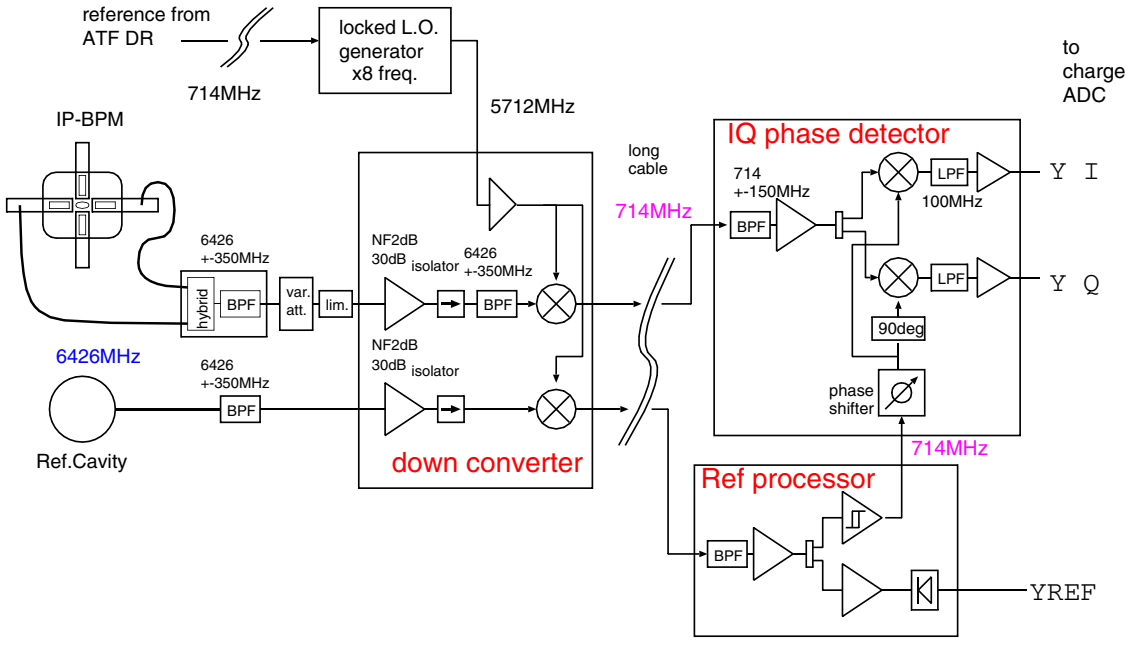

FIG. 10. (Color) Schematic diagram of the electronics. The C-band signal of the BPM cavity and the reference cavity are down-converted to 714 MHz at first. Then, the BPM signal was demodulated into I and Q components using the signal from the reference cavity as the phase reference.

down-converter module placed in the accelerator tunnel then converts the C-band signal into IF before transferring it through a cable about 30 m long. The first amplifier in the module dominates the noise figure (NF) in the overall system. We chose ones that are specified as 30 dB gain and 2 dB NF. A BPF of ± 350 MHz BW rejects the noise from the amplifier at the image frequency. The local oscillator (L.O.) used for the mixer is provided externally. A 714 MHz timing reference signal is provided by the ATF damping ring rf system. We expect that the beam in the extraction line is synchronized to this reference. It is used to generate the L.O. of 5712 MHz, which differs from the BPM signal by 714 MHz, through an 8th harmonics generator.

The signal from the reference cavity is processed similarly. A BPF is used to reject the other modes, and then the signal is fed to the down-converter module. Using the same external L.O., it is down-converted to 714 MHz while conserving the phase relation with the BPM signals.

At the electronics hut outside the accelerator tunnel, the IF signals from the BPM and the reference cavities are further processed using analog electronics. The Ref-processor module extracts the information in the beam charge (YREF) by rectifying the reference cavity signal with a diode detector. At the same time, it produces a beam-based phase reference of 714 MHz through a limiter amplifier. The phase shift in the produced reference signal depending on the input power is less than 10 degrees. This reference is used to detect the phase of the BPM signals. In the IQ phase detector module, the signal is split and sent to two mixers, and detected into the base band having orthogonal phases (I and Q). The bandwidth is determined by a 100 MHz low-pass filter placed after the mixer. The phase origin of the detection can be adjusted using the manual phase shifter at the input of the phase reference. The relative phase stability of the BPM signals was within 1 degree of the signal from the reference cavity.

The final output signals are YnI, YnQ, XnI, XnQ, YREF, and XREF ($n = 1, 2, 3$). They are recorded using 14-bit charge-sensitive analog-to-digital converters (ADCs). The effective bandwidth is determined by the gate width of the ADC, which is set to a width of 50 nsec starting 50 nsec after the leading edge of the pulse. The leading edge is intentionally avoided because that part of the signal might contain a transient signal from unwanted modes.

The sensitivity of the system was checked by measuring a cw dummy signal of an rf source with 20 MHz bandwidth at the output, which roughly corresponds to the 50 nanosecond wide gate. The minimum detectable power against thermal noise was estimated to be -95 dBm at the input of the down-converter. Signal attenuation between the BPM ports and the input of the down-converter was 6.6 dB. The decay time of the pulse was determined by the Q_L factor of the cavity. The signal voltage decayed to about 48% at the measurement timing of the ADCs, which reduced the effective position sensitivity. Considering all of the above together with the expected sensitivity of the BPM, which was estimated to be -104.5 dBm for 1 nm at the BPM output ports, the detection limit corresponded to the 3.0 nm position signal at the ATF's nominal beam.

B. Sensitivity control

Since the electronics are designed to have very high gain, their linear range corresponds to only about 5 μm around the center of the BPMs. This actually is smaller than typical beam position jitter at the beam line. In order to reliably calibrate the BPM, we scanned the beam in steps of about 100 μm, which was bigger than the beam jitter and drift. The variable attenuator placed in front of the down-converter module was used to switch the sensitivity and increase the dynamic range for calibration runs. The attenuator can be adjusted remotely in 10 dB steps. Its characteristics were bench tested in advance. The precision and phase shift were confirmed to be better than 0.5 dB and 30 degrees, respectively.

C. Phase tuning

The IQ phase detector has two outputs 90 degrees apart. By adjusting the phase shifter in the module, we set one of

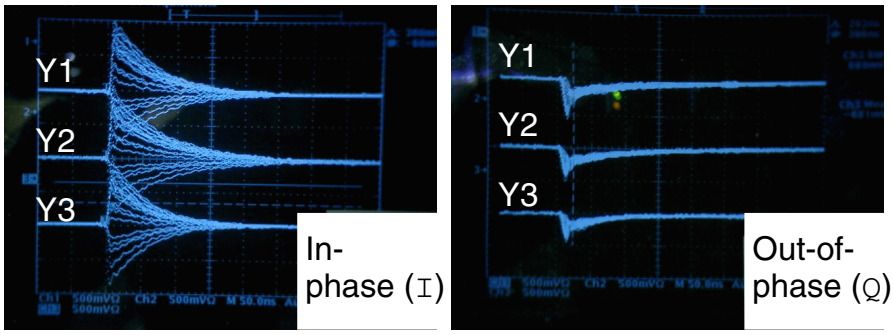

FIG. 11. (Color) Example of the output signals. After finishing the phase tuning procedure with a 30 dB attenuation setting, this example data was taken with 10 dB attenuation in the natural beam jitter. The scope was set to persistence mode, superposition of many pulses were shown in the picture. These pulses are recorded by charge ADCs.

the outputs, I, to be position sensitive and the other, Q, to be out of phase to output I. This was done in the following way. The variable attenuator was set to 30 dB in order to expand the dynamic range and relatively reduce the position-independent signals, such as the one simultaneously produced by the orbit angle. The beam orbit was scanned in parallel using a pair of steering magnets while monitoring the I and Q signals with an oscilloscope. The phase shifter was adjusted to minimize variation in the Q signals and maximize the I signals. Figure 11 shows an example after phase adjustment. The jitter in the beam position appeared mostly in the I signals.

D. Electronics performance test

A special run was carried out to estimate the resolution when limited by noise from the electronics. As shown in Fig. 12, the signal from a cavity was split into two sets of identical electronics. By comparing the results of signal detection in each set, the intrinsic performance of the electronics can be estimated without the complex effects of mechanical vibration, contamination by unwanted modes, etc. The data from the first set (Y1I and Y1Q) and the beam intensity (YREF) were used to predict the position signal in the second set (Y2I). The residual signal outside the predicted signal is system noise. The following linear model was used to make the prediction:

$$\mathrm{Y\,2I} = \alpha_{\mathrm{Y1I}}\mathrm{Y1I} + \alpha_{\mathrm{Y1Q}}\mathrm{Y1Q} + \alpha_{\mathrm{YREF}}\mathrm{YREF}. \qquad (12)$$

Coefficients α_x were determined by means of regression analysis to minimize the residual between the prediction and the measurement of many pulses. Measurements were taken at 4 different settings (0, 10, 20, and 30 dB) of the variable attenuator.

The sensitivity calibration run was done with 30 dB attenuation. The beam orbit was scanned in parallel using steering magnets while measuring the beam position at the BPM interpolated from positions of the stripline BPMs in the vicinity. The calibration factor for the other attenuator settings was calculated from that at 30 dB. The rms of the predicted residual signal was scaled using these calibration factors.

Because of the statistical factor of comparing two identical sets, the rms of the actual residual signal should be larger than the intrinsic noise by a factor $\sqrt{2}$. The 6 dB splitter used to divide the BPM signal reduced the signal by a factor of 2 as compared with the original configuration. The average beam charge in this run was 0.67×10^{10} e/bunch, while the specified nominal charge of the ATF is 1.0×10^{10} e/bunch. Therefore, the intrinsic resolution of the original setup at the nominal charge was estimated as follows:

$$\left(\frac{1}{\sqrt{2}}\right) \times \left(\frac{1}{2}\right) \times \left(\frac{\text{average charge}}{\text{nominal charge}}\right) \times \left(\frac{\text{rms of residual}}{\text{calibration factor}}\right).$$

The results of different attenuator settings are plotted in Fig. 13. We can expect 2.6 nm resolution at the nominal

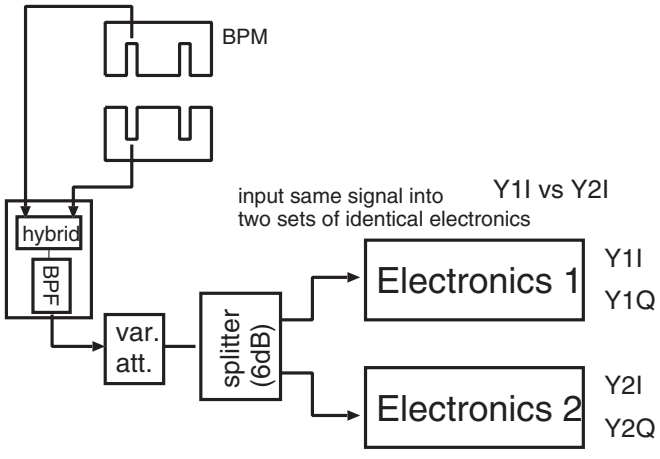

FIG. 12. Setup for testing intrinsic resolution of the electronics. Identical signals divided from one BPM were processed by two sets of electronics.

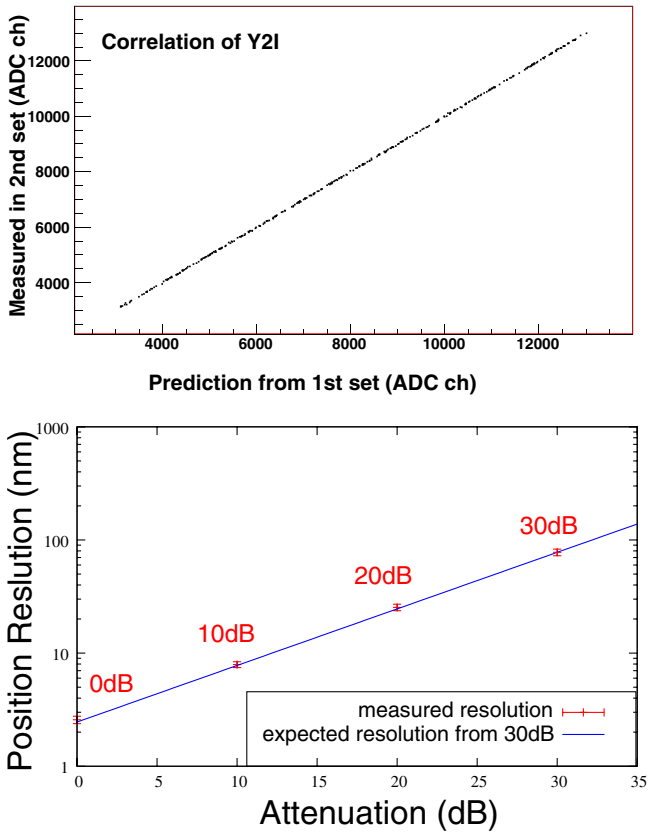

FIG. 13. (Color) Results of intrinsic resolution of the electronics. The scatter plot in the top shows the actual measurement result of Y2I. against the prediction of Y2I from Y1I, Y1Q, and YREF The resolution can be calculated from the distribution of the residual (width of the line). The bottom plot is the summary of various settings of the attenuator. Extrapolation from the data at 30 dB is shown as the line.

beam charge. This is consistent with the detection limit of the electronics when the attenuation is 0 dB. All of the data points were confirmed to be on the line extrapolated from the data at 30 dB. The electronics worked well even at high sensitivity settings, although there was concern that unwanted signals might be relatively larger in these cases.

VI. RESOLUTION MEASUREMENT

A. Data collection

The actual measurement of the resolution using three BPMs was done in a way similar to that done in the intrinsic resolution test of the electronics described in the previous section. At first, sensitivity calibration of each channel was done with 30 dB attenuation setting. The result is shown in Fig. 14. The ADC readout of each BPM are plotted as a function of the beam position calculated from interpolation of stripline BPMs. Fitting the data by a linear function produced the calibration factors needed to convert the ADC readouts to beam positions. To estimate systematic errors in the calibration factor, the calibration procedure was repeated several times and also

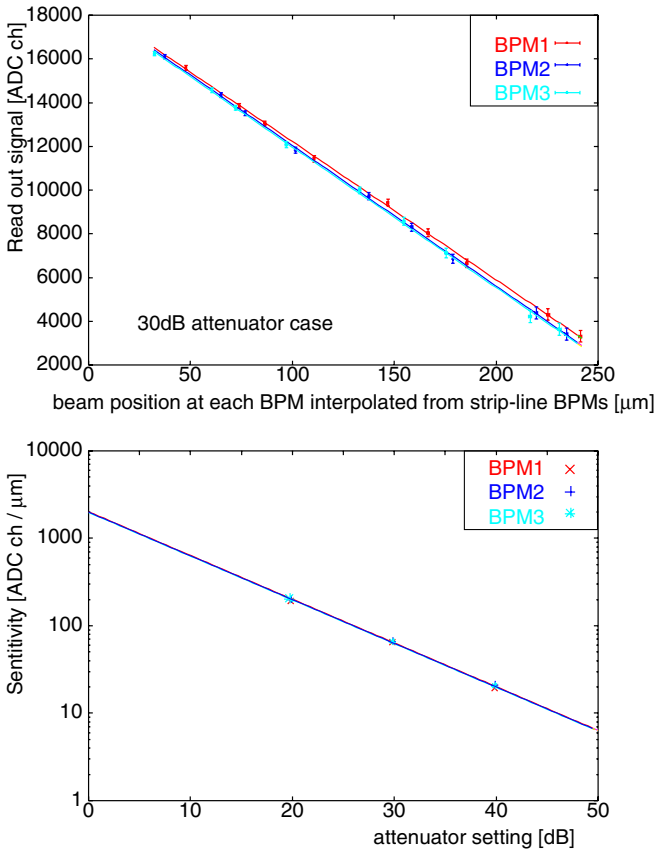

FIG. 14. (Color) Results of the calibration run. The top plot shows ADC readouts as a function of beam position for the three BPMs. Lines are the fitting results. Average and variation of the calibration results of repeated measurement are plotted in the bottom plot for various settings of the attenuator.

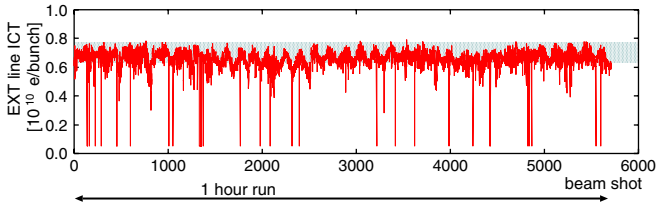

FIG. 15. (Color) Trend of beam intensity during a 1-hour run. Approximately 60% of the data survived the intensity cut.

with different variable attenuator settings of 20 and 40 dB. The bottom plot in Fig. 14 summarizes the results, which shows that the calibration results reproduced well and that changes in the expected line as a function of the attenuation. Although calibrations at attenuation settings of 0 and 10 dB were impossible due to the limited dynamic range, they are extrapolated from the calibration results for 30 dB attenuation.

Long runs, called resolution runs, were conducted with a fixed beam condition with various settings of the variable

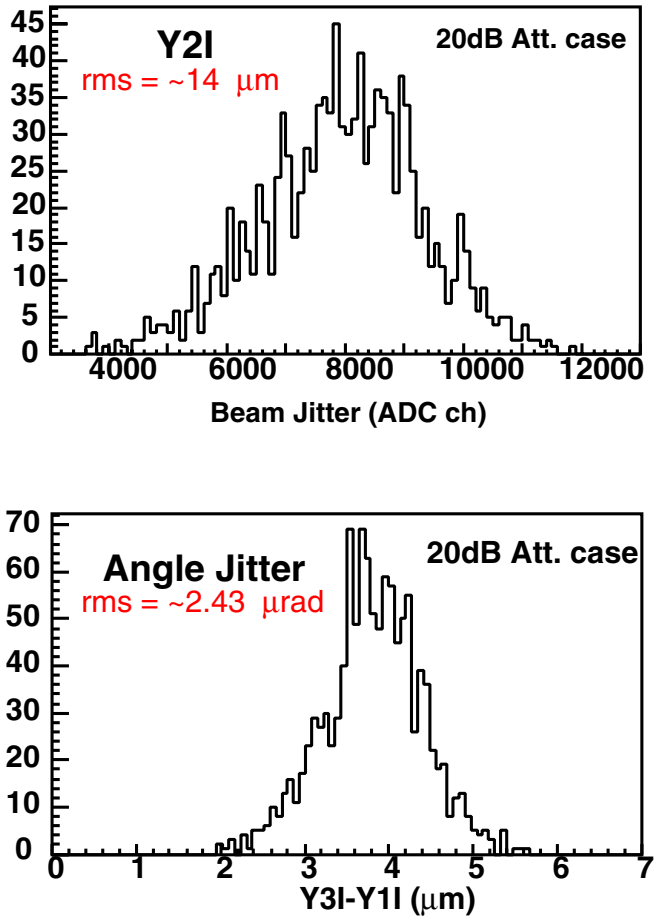

FIG. 16. (Color) Typical beam jitter. The top figure is the statistics of vertical beam position (Y) measured at the 2nd cavity BPM. The bottom figure is the vertical beam angle (Y′) tracked by 1st and 3rd cavity BPMs.

attenuator. Typically, 1000 beam pulses, about 10 min long, were collected from each run. To check the system's long term stability, a longer (1 h) run was also conducted.

In order to take data in a fixed condition, we set an intensity cut for all runs including the calibration runs. Prior to the experiment, the intensity readings from the reference cavity were calibrated with respect to the current transformer (CT) located at the end of the beam line. The intensity was cut by $0.65 \sim 0.75 \times 10^{10}$ electrons/bunch. Figure 15 shows the variation in the beam charge in a typical run. We guess the time structure in the beam intensity was caused by an environmental change in the accelerator. Figure 16 shows the distribution of the beam positions and angles measured by the cavity BPMs. There was a beam position jitter of $\sim$14 μm and a beam angle jitter of $\sim$2.7 μm in our experiment.

B. Resolution analysis

By comparing the data from the three BPMs, the intrinsic resolution of a BPM can be estimated. Two of the three, the first and third BPMs, are used to determine the beam orbit and predict the beam position at the second BPM. Since the beam jitter was larger than the dynamic range of the electronics, data outside the range of 5 μm at any BPM was rejected in the resolution analysis. The following linear model containing all available information was used to make the prediction:

$$\begin{aligned} \mathrm{Y2I} = {} & \alpha_{\mathrm{Y1I}}\mathrm{Y1I} + \alpha_{\mathrm{Y1Q}}\mathrm{Y1Q} + \alpha_{\mathrm{X1I}}\mathrm{X1I} + \alpha_{\mathrm{X1Q}}\mathrm{X1Q} \\ & + \alpha_{\mathrm{Y3I}}\mathrm{Y3I} + \alpha_{\mathrm{Y3Q}}\mathrm{Y3Q} + \alpha_{\mathrm{X3I}}\mathrm{X3I} + \alpha_{\mathrm{X3Q}}\mathrm{X3Q} \\ & + \alpha_{\mathrm{YREF}}\mathrm{YREF} + \alpha_{\mathrm{XREF}}\mathrm{XREF}. \end{aligned} \tag{13}$$

As long as the variations in the beam condition are small, we can assume that each term's contribution is linear. The coefficients, α_x, to minimize the residual were determined by regression analysis. The terms of Y1I, Y3I, and YREF are the main terms that used to determine the trajectory and normalize the beam charge. The contribution from the information in X is due mainly because of the relative alignment errors for the three cavities in the system. Considering the sensitivity difference due to the 30 dB signal attenuation intentionally added to the X signals for measuring bigger beam jitter, the relative sizes of the coefficients of the X terms with respect to those of the main terms in YI were smaller than 1%. The terms of the Q phase are included to correct the imperfections in-phase adjustment. The size of the coefficients of the YQ terms were compared with the main terms of YI by normalizing the deviations of each datum. The relative contribution of the YQ terms was less than 4%.

Figure 17 is a scatter plot of the predicted and the measured signals. The distribution of the residual signal, the width of data in the scatter plot, is shown in the bottom plot. Figure 18 shows the variation in the residual during a long run of 1 h duration. The data shows no significant drift

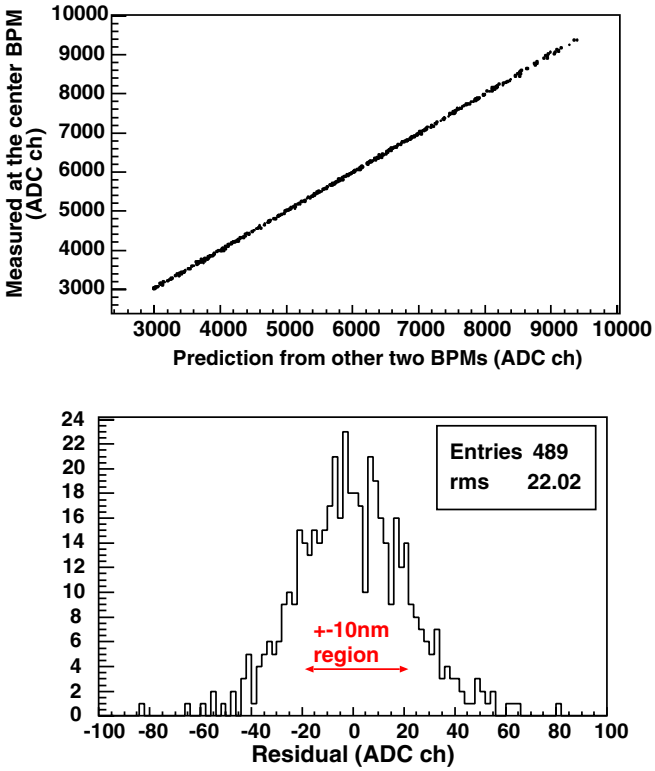

FIG. 17. (Color) Resolution measurement data. The top figure shows a scatter plot of the prediction and measurement. The bottom figure is the distribution of the residual of the prediction.

in the residual signal, proving the stability of the system, both in mechanically and electrically, at about the 10 nm level.

The intrinsic resolution of the BPM was estimated from the rms of the distribution using the following equation:

$$(\text{geometrical factor}) \times \left(\frac{\text{rms of residual}}{\text{calibration factor}}\right).$$

The statistical factor (geometrical factor) is given from the geometry noted in Fig. 6. The results at various attenuator settings are summarized in Fig. 19. At the highest sensi-

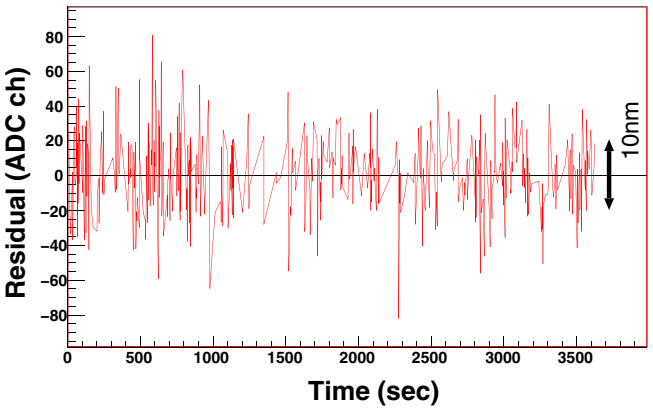

FIG. 18. (Color) Trend of the residual in a long run.

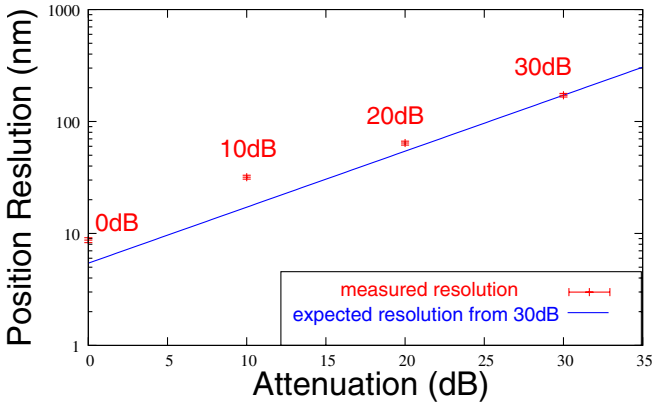

FIG. 19. (Color) Summary of resolution measurements with various settings of the variable attenuator. The line is the extrapolation from the data at 30 dB attenuation case.

tivity, 0 dB attenuation, the position resolution is $8.72 \pm 0.28(\text{stat}) \pm 0.35(\text{syst})$ nm, where the first error is the statistical error in determining the rms of the residual. The second error is the systematic error from the error in the calibration factor. The average beam charge in the data is 0.68×10^{10} electrons/bunch.

VII. DISCUSSION

The intrinsic noise of the system was estimated to be 2.6 nm at 10^{10} e/bunch. It is scaled to 3.8 nm at 0.68×10^{10} e/bunch. Subtracting this contribution from the proven resolution of 8.7 nm shows that 7.9 nm of unknown noise remains. The resolution goal of the position measurement for the ATF2 IP is a few nm. The origin of the unknown noise must be studied in order to further improve the resolution.

The temperature at various points, for example, at the BPM block, the air in the area, and at the electronics box, had been measured during the long runs. The environment turned out to be fairly stable within 10 mK, and the measurement was actually limited by the resolution of the sensor. The residual signals for the 3 BPM showed no clear correlations and provided no clues as to the source of the unknown noise.

Mechanical vibration was checked using a distance meter based on a laser interferometer. The motion of the BPM block with respect to the granite table was measured. The rms variation in the short time vibration turned out to be 4.3 nm, at the dominant frequency of about 40 Hz. Slow drift was not very significant in ~minute time scale. Note that this result includes any coherent motion of the whole system that does not degrade the resolution measurement.

Contamination of the common modes is difficult to estimate. Even if there is common-mode leakage, it only produces a constant shift of the electrical center. It does not affect the resolution result when its excitation is stable. Variations in bunch length might change the excitation of the common modes. A device to monitor the bunch length will be added in future.

A longitudinal tilt of the bunch can produce a quadrature-phase signal. Typical beam position jitter and trajectory angle jitter were estimated in Fig. 16 to be ~14 μm and ~2.4 μrad, respectively. From Fig. 11, the jitter in quadrature-phase component is estimated to be ~10% of the in-phase component. The jitter appearing in the quadrature phase is equivalent to a 1.4 μm position signal. It does not explain the trajectory angle signal discussed in Sec. IV D. If the quadrature component was originated by longitudinal bunch tilt, its jitter should be as much as ~3.2 mrad. At present, we have no good device to directly check the bunch tilt. If the bunch tilt somehow affects the signal, a device to check the bunch tilt may help us to investigate our problems.

So far, we have taken several sets of data, but generally, they were all obtained under fixed beam conditions. Tests to check the beam charge dependence of resolution and tests with different beam sizes and divergence in the area are planned.

VIII. CONCLUSION

This paper describes the development of a high-resolution cavity BPM. This BPM will be used at the virtual IP of the ATF2 beam line to measure beam jitter. The new cavity structure is optimized for our needs. For example, the rectangular shape isolates two dipole modes in the orthogonal direction and the thin gap reduces the sensitivity to trajectory inclination. The characteristics of the cavity were checked in beam tests. A highly sensitive analog processor with phase-sensitive detection was also developed. Beam tests at the existing ATF extraction line showed 8.7 nm position resolution for a 0.68×10^{10} e/bunch beam with a dynamic range of 5 μm. This is a better result than was achieved in past studies [1–4]. Although it is difficult to compare this study with studies using different beams, we note improvements we have made in this work. The unique shape of our cavity may have helped to extract a less-contaminated position signal. Measurement of all of the X and the Y direction data and I and Q phase data allowed us to use regression analysis to remove signal correlations. The rigid support and combined cavity block may have reduced mechanical motion in the system. A stable beam at the ATF extraction line may have helped also.

ACKNOWLEDGMENTS

We would like to express our gratitude to all the operators, collaborators, and support staffs in the ATF group. We acknowledge P. Bambade and P. Doublet of LAL for their contributions to the tests in the early stage. We would like to thank S. Walston, A. Lyapin, and the SLAC/LLNL/UK collaborators for fruitful discussions. The present work

was carried out with partial support from the "Grant-in-Aid for Creative Scientific Research of JSPS (KAKENHI 17GS0210)" project of the Ministry of Education, Science, Sports, Culture and Technology of Japan (MEXT). One of the authors (Junji Urakawa) received support from the Japan-USA Collaboration Research Grant from MEXT and from the Core-University Program of the JSPS. We also thank Professor J. M. Paterson of the ATF ICB Chair for supporting the ATF project as an international collaboration.

[1] V. Balakin *et al.*, *Proceedings of the Particle Accelerator Conference, New York, 1999* (IEEE, New York, 1999).
[2] T. Shintake, Report No. KEK-PREPRINT-98-188, 1998.
[3] T. Slaton *et al.*, Proceedings of the XIX International Linac Conference, Chicago, 1998, pp. 911–913.
[4] S. Walston *et al.* (to be published).
[5] F. Hinode *et al.*, KEK Internal Report No. 95-3, 1995.
[6] *ATF2 Proposal*, Report No. KEK-Report-2005-2.
[7] A. Lyapin, Dissertation, TU-Berlin, Berlin, 2003.
[8] M. Ross *et al.*, *Proceedings of the Particle Accelerator Conference, Portland, OR, 2003* (IEEE, New York, 2003), pp. 2548–2550.
[9] Z. Li *et al.*, Proceedings of the Particle Accelerator Conference, Portland, OR, 2003, Ref. [8].
[10] MAFIA is an electromagnetic field simulator. http://www.cst.com/Content/Products/MAFIA/Overview.aspx.
[11] HFSS is an electromagnetic field simulator. http://www.ansoft.com/products/hf/hfss/.
[12] H. Hayano, Proceedings of the 20th International Linac Conference, Monterey, CA, 2000.